Bulletin of the Seismological Society of America, Vol. 86, No. 2, pp. 371–378, April 1996

Low-Velocity Fault-Zone Guided Waves: Numerical Investigations of Trapping Efficiency

by Yong-Gang Li and John E. Vidale*

Abstract Recent observations have shown that shear waves trapped within low-velocity fault zones may be the most sensitive measure of fault-zone structure (Li *et al.,* 1994a, 1994b). Finite-difference simulations demonstrate the effects of several types of complexity on observations of fault-zone trapped waves. Overlying sediments with a thickness more than one or two fault-zone widths and fault-zone step-overs more than one or two fault widths disrupt the wave guide. Fault kinks and changes in fault-zone width with depth leave readily observable trapped waves. We also demonstrate the effects of decreased trapped wave excitation with increasing hypocentral offset from the fault and the effects of varying the contrast between the velocity in the fault zone and surrounding hard rock. Careful field studies may provide dramatic improvements in our knowledge of fault-zone structure.

Introduction

Major crustal faults are often marked by zones of lowered velocity with a width of a few hundred meters to a few kilometers (Healy and Peake, 1975; Feng and McEvilly, 1983; Mooney and Ginzburg, 1986; Li and Leary, 1990; Scholz, 1990; Michelini and McEvilly, 1991). These low-velocity zones are thought to be caused by an unknown combination of fluid concentrated near faults, clay-rich fault gouge, increased porosity, and dilatant cracks (Sibson, 1977; Wang, 1984; Li *et al.,* 1990). The strength of the low-velocity anomalies might vary over the earthquake cycle (Li *et al.,* 1994a). Recently, fault-zone guided waves have been shown to reveal detailed information about the fine structure at the heart of fault zones and its lateral variation (Li *et al.,* 1994a, 1994b). Since fault-zone trapped waves arise from constructive interference of multiple reflections at the boundaries between the low-velocity fault zone and high-velocity surrounding rocks, the feature of trapped waves (including amplitudes and frequency contents) are strongly dependent on the fault-zone geometry and physical properties. We can resolve fault-zone width from tens to several hundreds of meters using the records of fault-zone trapped waves. It is of interest to determine the factors that influence the propagation of these waves.

The fine structure of fault zones is of great interest because the factors that control the initiation, propagation, and termination of rupture are not well understood (Aki, 1984; Scholz, 1990; Kanamori, 1994). Rupture models have been proposed that involved variations in fluid pressure over the earthquake cycle (Sibson, 1973; Blanpied *et al.,* 1992). Other studies predict that most earthquake energy is stored in areas with less-developed fault zones (Mooney and Ginzburg, 1986) or with higher-velocity rock outside the fault zone (Michael and Eberhart-Philips, 1991; Nicholson and Lees, 1992). Observations suggest that fault-zone complexity may segment fault zones (Lindh and Boore, 1974; Aki, 1979; Beck and Christensen, 1991) or control the timing of moment release in earthquakes (Campillo and Archuleta, 1993; Harris and Day, 1993; Li *et al.,* 1994a, 1994b; Wald and Heaton, 1994). For all these models, knowledge of lateral variations or temporal variations in fault structure will help predict the behavior of future earthquakes, and such knowledge will help evaluate the models as well.

Faults also sometimes mark the boundary between types of rocks with distinct seismic velocities, but the resulting refracted arrivals (McNally and McEvilly, 1977; Ben-Zion and Malin, 1991) are beyond the scope of this article.

The Simulation Method

We use finite-difference simulations below to investigate the effects of various possible fault structures as well as structures that might obscure the signature of faults. The finite-difference code is acoustic, fourth order in time, second order in space, and two-dimensional (Alterman and Karal, 1968; Vidale *et al.,* 1985; Vidale, 1990). The *SH*-wave equation is solved, and we are examining the component of *S* motion parallel to the strike of the fault. Windowing based on the precalculation of travel times by a

*Present address: Department of Earth and Space Sciences, University of California, Los Angeles, Los Angeles, California 90095-1567.

finite-difference eikonal method (Vidale, 1988) reduces the computational requirements by a factor of 4.

Each calculation uses a 600-by-600 element grid to simulate a vertical cross section that strikes perpendicular to the surface trace of the fault. The grid spacing is 20 m. The minimum velocity in the simulations is usually 2 km/sec, and we use a time step of 0.008 sec (Alford *et al.,* 1974). We use at least eight grid points per wavelength to minimize grid dispersion (Alford *et al.,* 1974). The fault zone is placed down the middle of the grid, far enough from the left and right edges that side reflections do not appear in the seismograms. The sources are shallow enough that bottom reflections also arrive later than the arrivals we analyze. The top surface, where the seismometers are located, is a free surface.

The simulation is for a line source; to simulate a point source, we apply an approximate correction. The time series in each seismogram is differentiated with respect to time t and convolved with the time series $1/\sqrt{t}$ (Vidale *et al.,* 1985). An isotropic radiation pattern is used, although in earthquakes, the familiar P and S radiation patterns of a double couple are present (Aki and Richards, 1980). In elastic finite-difference modeling of strong motion records from the 1971 San Fernando earthquake, Vidale and Helmberger (1987) have shown that despite the three-dimensional nature of the basins, the geometry may be approximated by a two-dimensional model with useful results. They, however, note that the amplitude attenuation due to geometrical spreading in the two-dimensional profile may vary somewhat due to three-dimensional effects, even if the energy path is not laterally deflected. They also note that the simulations of the energy in nodal directions may be a problem. We note that in our previous work (Li *et al.,* 1994b) the appropriate double-couple radiation patterns were included. In the present article, we illustrate an example of seismograms using the double-couple source with the S radiation pattern (Fig. 9) and compare with seismograms using isotropic radiation pattern.

Previous articles have used analytical methods to compute seismograms that result from layer-cake fault models (Li *et al.,* 1987) or raytracing methods that are limited by the difficulty of finding ray paths in strongly heterogeneous structures (Cormier and Spudich, 1984). This study provides the next logical step by allowing arbitrary velocity variations in a two-dimensional cross section, with the limitation that no along-strike variation is allowed, and the source and receiver must be in the same cross section that is perpendicular to the fault. The computation of fault-zone trapped waves with 3D elastic structures has been demonstrated, but so far only propagation to a distance up to several wavelengths has been obtained with a Connection Machine (Igel *et al.,* 1991; Leary *et al.,* 1991).

Simulation Results

The Reference Model

Our simulations are based on geometries similar to those inferred for major vertical strike-slip California faults (Li *et al.,* 1994b). In the simulations, our reference model has an 8-km source depth, the fault-zone width is 200 m, and the source is placed against one edge of the low-velocity fault zone. The receiver array is centered on the surface fault trace. We set the wall rock shear-wave velocity to 3 km/sec and the fault zone velocity to 2 km/sec, so the velocity anomaly in the fault zone is about 40%. This structure most effectively traps 3- to 10-Hz shear waves.

The Perturbations to the Reference Model

Table 1 lists the model parameters used in various fault structures, and maximum amplitudes of the seismograms generated with these fault models as well as the figure numbers in which seismograms are shown.

Effect of Source Location

Guided waves are most efficiently excited by a seismic source that is located within the wave guide. This is clear in Figure 1, which shows the ground motion for no wave guide (Fig. 1a) and for five source positions at various distances from the wave-guide center. The maximum amplitude of seismograms generated in each case is listed in Table 1. The sources in the center (Fig. 1b) and on the edge of the fault zone (Fig. 1c) produce large guided waves. The centered source location produces less high-frequency trapped energy because of the symmetric source radiation pattern and symmetric fault structure. There are no numerical problems with the edge of the fault zone. However, a real fault would contain attenuation and heterogeneity that may mask the differences between source locations within the fault zone.

A source location 200 m, or one fault-zone width, outside the fault zone (Fig. 1d) still produces visible trapped waves that appear within a few hundred meters of the fault trace. However, their amplitude is about a factor of 3 weaker than for source locations inside the fault zone. A source 400 m outside the fault (Fig. 1e) excites only the longest-period guided waves. A source 1000 m outside the fault (Fig. 1f) produces no guided waves, although some reflections and shadowing from the sides of the fault zone are still visible.

Effect of Fault-Zone Width and Velocity Contrast

The amount of reduction of velocity in the fault zone determines the amount of dispersion in the guided wave. A 20% velocity reduction (Fig. 2a) results in a more compact guided wave than a 50% velocity reduction (Fig. 2b). The frequency content of the guided wave also depends on the velocity within the fault zone, since lower-velocity material within a fixed width fault zone causes longer-period resonance, but this effect is weak.

The width of the low-velocity fault, however, controls the frequency of the guided waves. An 80-m-wide fault zone shows a clear shift toward higher-frequency guided waves (Fig. 2c) compared with the reference model of a 200-m-wide fault zone (Fig. 2b).

Table 1
Perturbations in Model Parameters and Maximum Amplitudes

Reference Model Parameters:						
Fault-zone thickness:	200 m					
Fault-zone velocity:	2.0 km/sec					
Wall rock velocity:	3.0 km/sec					
Source depth:	8.0 km					
Number of receivers:	31					
Receiver space:	40 m					
Array length:	1.2 km					
Array position:	centered on the surface fault trace					
Source Position: (offsets from the center of the fault zone)						
Source offset (m):	0	0	100	300	500	1100
Fault-zone velocity (km/sec):	3	2	2	2	2	2
Maximum amplitude:	0.3055	3.9829	2.5941	0.5719	0.4075	0.6215
Figure number:	1a	1b	1c	1d	1e	1f
Fault-Zone Width and Velocity Contrast:						
Fault-zone velocity (km/sec):	2.5	1.8	2.0			
Fault-zone thickness (m):	200	200	80			
Maximum amplitude:	3.2891	3.5119	1.5625			
Figure number:	2a	2b	2c			
Thickness of the Surface Layer:						
Surface-layer velocity (km/sec):	1.5	1.5	1.5			
Layer thickness (m):	200	600	1000			
Maximum amplitude:	3.6208	3.0158	2.2454			
Figure number:	3a	3b	3c			
Depth of the fault top (m):	100	200	600			
Maximum amplitude:	3.5784	3.2174	2.3842			
Figure number:	3d	3e	3f			
Kink in the Fault Zone:						
Fault kink at a depth of 4 km.						
Fault bent from the vertical (°):	15	30	45			
Maximum amplitude:	2.8609	3.1867	1.6935			
Figure number:	4a	4b	4c			
Variable Width in the Fault Zone:						
Fault width at surface (m):	200	320	80			
Fault width at source depth (m):	200	160	160			
Maximum amplitude:	3.9829	2.5411	2.3666			
Figure number:	5a	5b	5c			
Fault Branch:						
Two branches are 800 m apart from each other at surface and connected at a depth of 4 km.						
Widths of two branches (m):	200 and 200	200 and 80				
Maximum amplitude:	2.1008	2.9056				
Figure number:	6a	6b				
Distance between the two branches at depth (m):	1000					
Depths of two fault kinks bent at 45° (km):	3, 4					
Maximum amplitude:	0.9211					
Figure number:	6c					

Table 1
Continued

Fault Step-over:			
Fault step-over at a depth of 4 km.			
Step distance (m):	200	500	1000
Maximum amplitude:	1.5567	1.1959	1.1548
Figure number:	7a	7b	7c
Fault-Zone Depth:			
Depth of the fault bottom (km):	7	4	2
Maximum amplitude:	2.1706	1.3171	0.8563
Figure number:	8a	8b	8c
Source Radiation:			
Velocity of fault zone (km/sec):	2.0	2.0	
Velocity of wall rock (km/sec):	2.0	3.0	
Source offset (m):	0	100	
Figure number:	9a	9b	

Effect of a Surface Layer

The closer that the low-velocity fault zone approaches the surface, the more clearly fault-zone guided waves appear at the fault trace. This tendency is shown by three simulations with a 200-, 600-, and 1000-m-thick layer (Figs. 3a, 3b, and 3c) with 1.5 km/sec shear-wave velocity on top of our standard fault model, which is 200-m wide. The simulation with 200 m of slow material atop the bedrock preserves most of the characteristics of the simulation where the fault reaches the surface (Fig. 1b). However, 1000 m of cover significantly distorts and attenuates the guided waves. This factor may make the characterization of fault zones difficult beneath sedimentary basins or other fault geometries that do not reach the surface. Figures 3d, 3e, and 3f show simulations for the fault zones buried at depths of 100, 200, and 600 m, respectively, in a simple half-space. Fault-zone guided waves are distorted and attenuated more seriously by the higher-velocity materials atop the fault zone than the lower-velocity materials due to the higher contrast between the velocity of fault zone and the velocity of surface layer. Downhole measurements may be desirable in the face of these complications.

Effect of a Kink in the Fault Zone

Since a fairly wide range of angles critically reflect from the 30% velocity contrast in our simulations, the effect of a kink is minor compared to the other structural complications we consider in this article. We bend the lower part of the fault 15°, 30°, and 45° from the vertical at the depth of 4 km (Figs. 4a, 4b, and 4c), while leaving the upper fault as vertical. The receivers remain centered on the surface fault trace. Only a minor loss in the amplitude of the guided waves is seen even for the fault with the 45° bend. The more visible difference is that there is a first-arriving direct shear wave for the greater kinks that travels straight through the bedrock. Also, the bigger kinks produce longer travel paths along the fault, which result in later fault-zone guided arrivals.

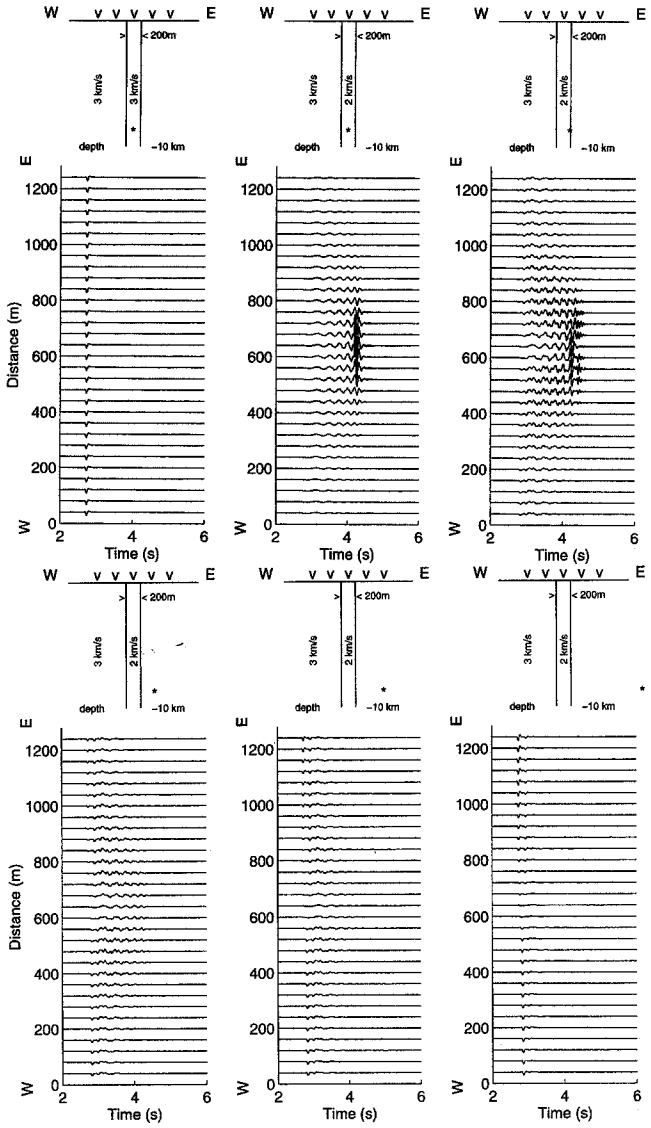

Figure 1. The effect of source location relative to a low-velocity fault on a profile of seismometers run perpendicular to the fault. The fault-parallel horizontal component is shown. The profile of Figure 1a shows the motions for a simple half-space. Frames (b), (c), (d), (e), and (f) show the motions for a source 0, 100, 300, 500, and 1100 m, respectively, from the center of the fault zone. A schematic diagram at the top of each frame shows the geometry of source (*), receiver array (v), and fault zone. The detail model parameters are listed in Table 1.

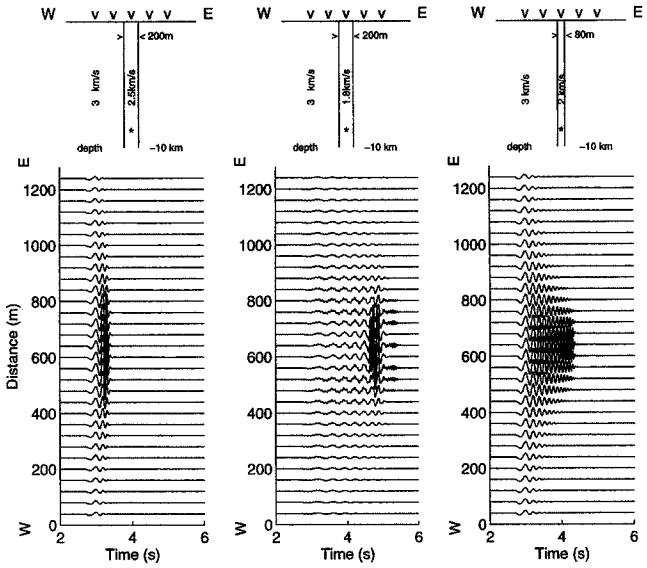

Figure 2. The effect of varying the fault-zone width and velocity contrast. The left profile shows motions for a fault zone with velocity 2.5 km/sec, the central frame shows motions for a fault zone of 1.8 km/sec, and the right frame shows motion for a fault zone only 80-m wide. Our reference model is 200-m wide with a velocity of 2 km/sec. Other notations as in Figure 1.

Effect of Fault Width Varying with Depth

As the factors that influence the creation and growth of the low-velocity material near the fault plane are not completely understood, it is possible that the fault-zone width may vary with depth. In all likelihood, the velocity within the fault zone also varies with depth, but this variation is probably less important than variations in the width.

We compare three models to quantify the effect of variable fault width. The original model (Fig. 5a) is compared with models that double in thickness from 160 to 320 m from the source depth to the surface (Fig. 5b) and that decrease by half in thickness from 160 to 80 m (Fig. 5c). Some differences in the dispersion are visible. The constant width fault has slightly larger guided waves. The trapped waves in the variable width zones show lower frequencies with the wider surface trace (Fig. 4b) and higher frequencies with narrower surface traces (Fig. 4c).

These fairly major variations in fault-zone width do not inhibit the propagation of fault-zone guided waves. It is clear that there is some information in the dispersion to constrain the depth variation of the fault-zone properties, but we will not examine the question of how much structure can be derived from a profile of *SH* motions from a single earthquake.

Effect of a Fault Branch

There are often multiple traces of faults at the surface, which may merge at depth or may remain parallel to seismogenic depths. Fault-zone guided waves may be a tool to probe the depth extent of such multiple traces or may be disrupted by such branching.

We examine the model shown in Figure 6a, which splits into two branches at a depth of 4 km. It is clear that some guided energy is partitioned into each branch, and the continuity of the wave guide is apparent from the seismograms (Fig. 6a). While, in general, branching fault traces may have very different wave-guide properties, abrupt branches, as in this example with identical wave guides above and below the junction, permit significant guided waves to cross the junction. Figure 6b shows, for example, simulations with

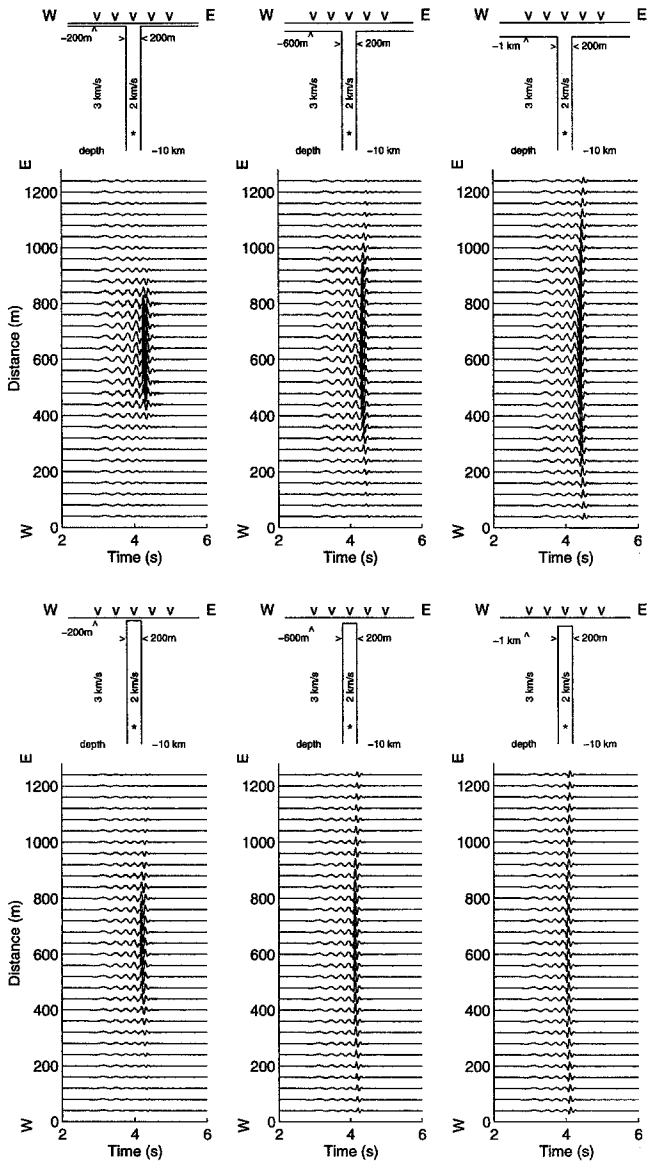

Figure 3. The effect of capping the low-velocity fault zone with an even surface layer. The three frames in Figures 3(a), (b), and (c) show the result of 200-, 600-, and 1000-m-thick surface layers, respectively, with velocity of 1.5 km/sec. Frames d, e, and f show the result from the fault zones buried at depths of 100, 200, and 600 m, respectively, in a simple half-space. Other notations as in Figure 1.

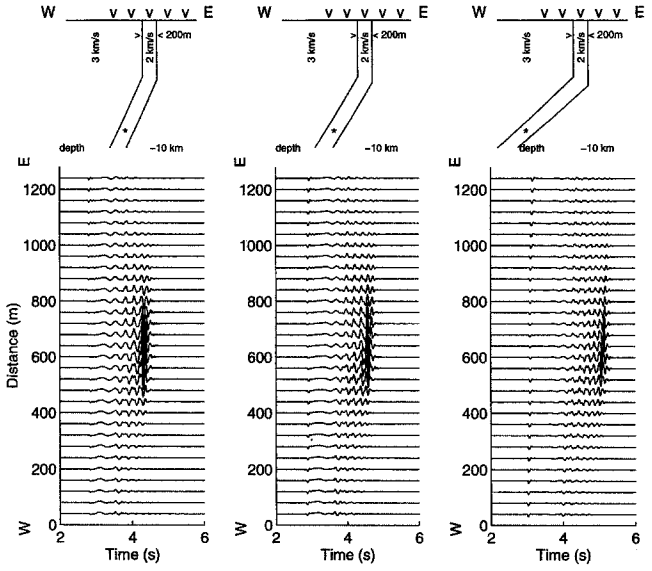

Figure 4. The effect of the fault kink at a depth of 4 km. The upper part of the fault remains vertical, and the profile is centered on the surface trace of the fault. The three frames show faults included 15°, 30°, and 45° to the vertical. Other notations as in Figure 1.

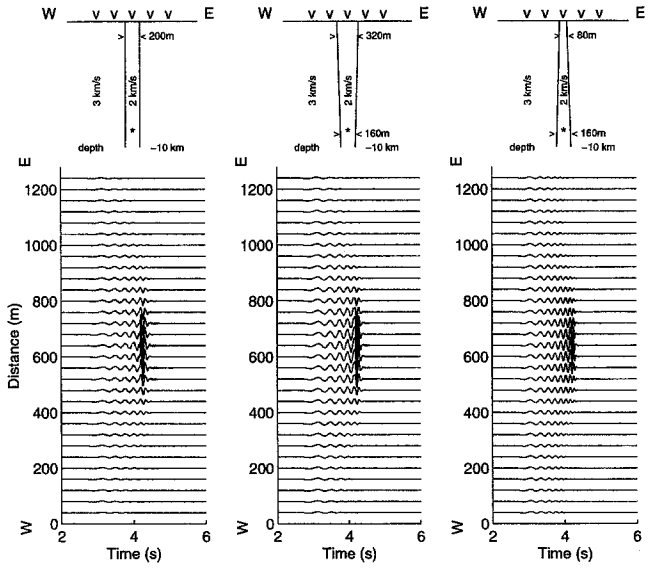

Figure 5. The effect of tapering the fault-zone width with depth. The left profile shows our reference simulation. The central profile shows a moderate taper from 320 m at the surface to 160 m at the source depth. The right profile shows a taper from 160 m at the source to 80 m at the surface. Other notations as in Figure 1.

two branches having different widths. The narrower branch with a width of 80 m produces higher-frequency guided waves than the 200-m-wide branch.

Effect of a Lateral Offset in the Fault Zone

It has been periodically suggested that horizontal detachments may offset shallow fault zones from deeper fault zones (Brocher *et al.,* 1994; Hadley and Kanamori, 1977; Louie *et al.,* 1988). While the details of such potential structures remain speculative, we present one case of the propagation of guided waves through a significant lateral offset.

Our horizontal jog model is vertical up to a depth of 4.5 km, bends to 45° from vertical up to a depth of 3.5 km, which results in 1 km of lateral offset, then continues vertically to the surface. In Figure 6c, it is apparent that some trapped energy propagates to the surface, having following the fault zone through both kinks, but the peak energy is reduced by

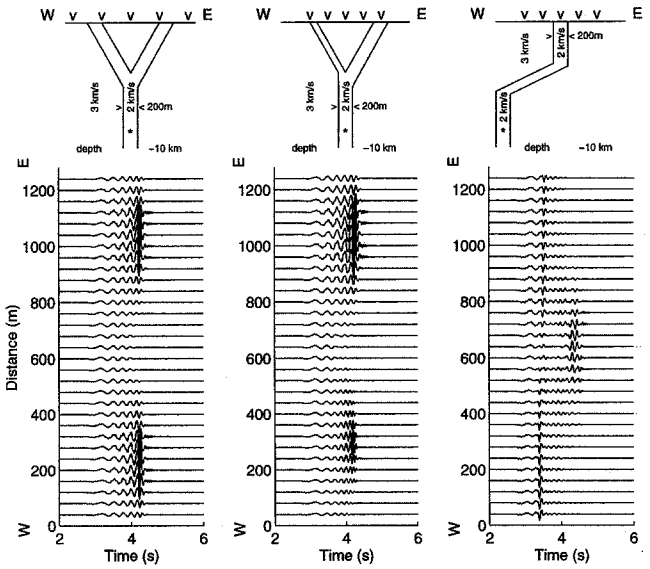

Figure 6. The effect of exotic structures. The left profile is the result of a fault that splits into two branches at a depth of 4 km. The right profile has a fault zone that is vertical from the source depth of 8 km up to 4.5 km, then it kinks to 45° from the vertical up to 3.5 km in depth, then it extends vertically to the surface. Other details are in Table 1. Other notations as in Figure 1.

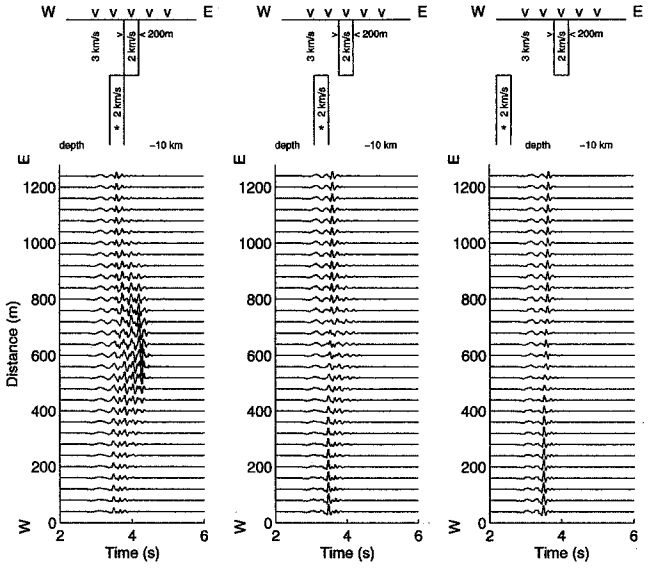

Figure 7. The effect of a fault-zone step-over. Frames (a), (b), and (c) show the results of a 200-, 500-, and 1000-m step-over, respectively, in the fault zone at 4 km in depth. There is no low-velocity material between the offset fault zones. Other notations as in Figure 1.

a factor of about 4 from that for a simple fault zone, as in Figure 1b.

Effect of a Fault Step-over

Seismicity studies of aftershocks for earthquakes with long ruptures suggest that fault surfaces may often consist of several simple but disjoint planes. The estimation of the width of the step-overs may be crucial in predicting the extent of future earthquakes (Harris and Day, 1993), specifically in guessing the structures that segment long faults. The lack of a continuous wave guide for the Landers fault zone, for example, has been linked to hesitation in the progression of rupture north along the fault during the Landers mainshock (Li *et al.*, 1994a, 1994b).

Figure 7 compares the effect of stepping the fault over by 200, 500, and 1000 m at a depth of 4 km. There is no low-velocity fault across the step-over. The smallest step-over, which is the same distance as the width of the fault, allows a lot of wave-guided energy to proceed up the fault zone. The largest step-over effectively blocks the wave guide. So stepping over much more than one fault zone width or, equivalently, stepping over several wavelengths of the fault-guided waves should result in the disappearance of the guided waves.

Effect of the Fault-Zone Depth

The depth to which a fault zone penetrates the crust is usually not well known. Some discrepancies exist in the fault-zone depth estimates in early studies of the San Andreas fault using seismological and gravity methods (Mooney and Ginzburg, 1986). Recently, using the fault-zone trapped wave data, Li *et al.* (1994a, 1994b) find that the fault zone ruptured in the Landers earthquake of 1992 may extend from the surface to a depth of at least 10 km, coinciding approximately with the lower limit of the seismogenic layer in the Mojave block.

We examine the effect of the fault-zone depth on the excitation and propagation of guided waves. Figure 8 shows three simulations with the fault zone depths of 7, 4, and 2 km. The source is located at a depth of 8 km beneath the fault zone. The simulation with 7 km of fault zone depth preserves most of the characteristics of fault-zone guided waves, as shown in Figure 1c. But the amplitude of fault-zone guided waves are reduced by a factor of 2, compared with Figure 1c. The fault zone with a depth of 4 km, however, results in a weaker and less dispersed guided wave than the deeper fault zone. In Figure 8c, only a short guided wave train is seen for the fault zone receivers if the fault zone penetrates the crust only 2 km.

Effect of the Source Radiation Pattern

So far in this article, we have used an *S* source that radiates isotropically for simplicity. Earthquakes radiate *S* waves with more complicated patterns. Strike-slip events on the vertical faults in California have been observed to excite trapped waves in nodal directions, so an example of the effect of radiation pattern is appropriate.

The radiation pattern of a dislocation point source used in this article is inserted by introducing "pseudo-near-field" terms that have permanent displacement near the source (Vi-

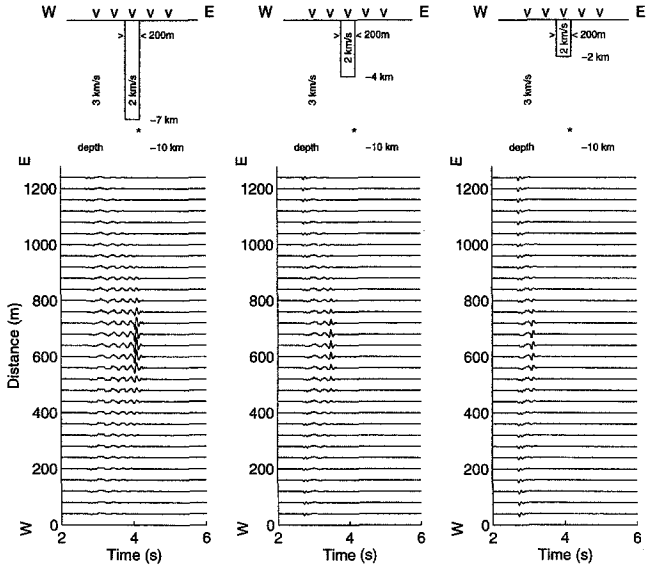

Figure 8. The effect of the fault-zone depth. The fault zones in (a), (b), and (c) extend from the surface to a depth of 7, 4, and 2 km, respectively, Other notations as in Figure 1.

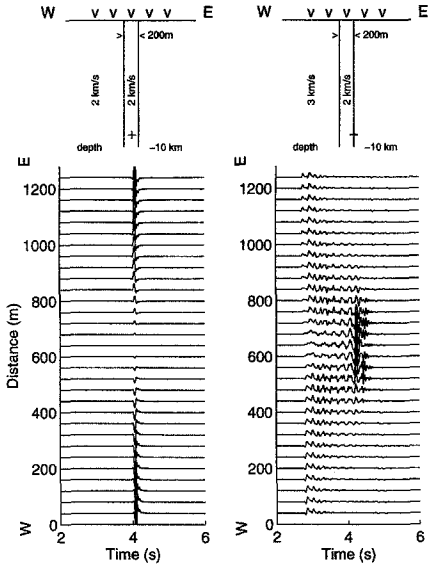

Figure 9. The effect of the source radiation pattern. The profile of (a) shows the motions for the double-couple source with *S* radiation pattern in a simple half-space. (b) shows guided waves excited by this source located against one edge of the low-velocity fault zone. Other notations as in Figure 1.

dale *et al.,* 1985). Figure 9 shows the ground motion for a double-couple source in the simple half-space without wave guide and for the source located at the edge of the low-velocity fault zone. It is clear that the *S* radiation pattern is created by the double-couple source (Fig. 9a). There is no significant difference in characteristics of fault zone guided waves between the source with and without the *S* radiation pattern (Fig. 9b and Fig. 1c).

Modeling Limitations

We have not addressed the effect of attenuation, coupled *P-SV* guided waves, or the guiding of *P* waves. We have assumed no variations in structure in the third dimension. We did not explore the effect of adding random heterogeneity to the fault zone or wall rock. The fault zone is modeled as a layer, while it is equally likely that the zone has gradational edges, such that rock properties approach those of the wall rock as one looks farther away from the fault zone. Some of these effects are likely to be important, but the first step, taken in this article, is to discuss the most basic influences on the propagation of fault-zone guided waves.

We feel further modeling efforts will be most fruitful in conjunction with examination of data from dense, 3-component deployments across faults, which can provide feedback about which fault models match real fault zones.

Conclusions

Low-velocity zones that are continuous from earthquakes to seismometers produce clear guided arrivals. The percentage velocity anomaly can be easily estimated to first order by measurement of the amount of delay of the slow arrivals. The width of the low-velocity channel can be easily estimated to first order by measurement of the frequency content of the delayed arrivals. These techniques have been applied to several faults in the last few years (Li *et al.,* 1990, 1994a, 1994b).

A flexible modeling technique like finite differences is required to judge the influence of the various structure that might be present. Some cases may require fully three-dimensional techniques, which are not yet routinely used (Igel *et al.,* 1991) to simulate the nearly 100-wavelength propagation distances at which fault-zone guided waves have been observed.

In this article, several rules of thumb are provided for the placement of fault-sensitive instrument deployments and interpretation of their results. Lack of sedimentary cover over the fault zone seems necessary. Hypocentral location within a few fault-zone widths of the fault is also necessary. Fault-zone continuity is also necessary. Other structural complexities have less effect. Bends, moderate changes in fault-zone width, and even bifurcating faults do not prevent the passage of guided waves.

By this exploration of the effect of structures on guided waves, it is clear that the identification of fault-zone width and percentage velocity anomaly requires at least several instruments recording several earthquakes in differing locations. Determination of more detailed fault structure requires many earthquakes, many stations in the fault-spanning array, and preferably several array installations; a volume of data that so far has only been gathered for Landers aftershocks (Li *et al.,* 1994a, 1994b).

The possibility of mapping the structures that are at the core of seismically active faults makes this effort worthwhile. Fault-zone guided waves are probably the only alternative to expensive drilling for imaging fault-plane fine structure. Such data are necessary to develop a well-based model of how earthquakes rupture.

Acknowledgments

We thank Robert Clayton for creating the first version of the finite-difference computer code. We also thank Kei Aki, Peter Leary, Walter Mooney, Paul Spudich, Heidi Houston, Ruth Harris, and H. M. Iyer for their helpful comments on the manuscript. Yong-Gang Li is supported by NSF Grant EAR-9404762 and the Southern California Earthquake Center under National Science Foundation Grant EAR-8920136 and U.S. Geological Survey Grant 14-0A-0001-A0899. This paper is SCEC publication 284.

References

Aki, K. (1979). Characterization of barriers on an earthquake fault, *J. Geophys. Res.* **84,** 6140–6148.

Aki, K. (1984). Asperities, barriers, characteristic earthquakes, and strong motion prediction, *J. Geophys. Res.* **89,** 5867–5872.

Aki, K. and P. G. Richards (1980). *Quantitative Seismology: Theory and Methods,* W. H. Freeman, San Francisco, California.

Alford, R. M., K. R. Kelley, and D. M. Boore (1974). Accuracy of finite-difference modeling of the acoustic wave equation, *Geophysics* **39,** 834–842.

Alterman, Z. and F. C. Karal (1968). Propagation of elastic waves in layered media by finite-difference methods, *Bull. Seism. Soc. Am.* **58,** 367–398.

Beck, S. L. and D. H. Christensen (1991). Rupture Process of the Feb. 4, 1965, Rat Islands earthquake, *J. Geophys. Res.* **81,** 1726–1736.

Ben-Zion, Y. and P. E. Malin (1991). San Andreas fault zone head waves near Parkfield, California, *Science* **251,** 1592–1594.

Blanpied, M. L., D. A. Lockner, and J. D. Byerlee (1992). An earthquake mechanism based on rapid sealing of faults, *Nature* **359,** 574–576.

Brocher, T. M., J. McCarthy, P. E. Hart, W. S. Holbrook, and K. Furlong (1994). Seismic evidence for a lower crustal detachment beneath San Francisco Bay, California, *Science* **265,** 1436–1439.

Campillo, M. and R. Archuleta (1993). A rupture model for the 28 June 1992 M 7.4 Landers, California, earthquake, *Geophys. Res. Lett.* **20,** 647–650.

Cormier, V. F. and P. Spudich (1984). Amplification of ground motion and waveform complexity in fault zones: examples from the San Andreas and Calveras faults, *Geophys. J. R. Astron. Soc.* **79,** 411–424.

Feng, R. and T. V. McEvilly (1983). Interpretation of seismic reflection profiling data for the structure of the San Andreas fault zone, *Bull. Seism. Soc. Am.* **73,** 1701–1720.

Hadley, D. and H. Kanamori (1977). Seismic structure of the Transverse Ranges, California, *Geol. Soc. Am. Bull.* **88,** 1469–1478.

Harris, R. A. and S. M. Day (1993). Dynamics of fault interaction: parallel strike-slip faults, *J. Geophys. Res.* **98,** 4461–4472.

Healy, J. H. and L. G. Peake (1975). Seismic velocity structure along a section of the San Andreas fault near Bear Valley, California, *Bull. Seism. Soc. Am.* **65,** 1177–1197.

Igel, H., P. Mora, D. Dominiques, P. C. Leary, and Y. Ben-Zion (1991). Finite difference simulation of fault zone trapped waves on the massively parallel connection machine (abstract), *EOS* **72,** 307.

Kanamori, H. (1994). Mechanics of earthquakes, *Annual Rev. Earth Planet. Sci.* **22,** 207–237.

Leary, P. C., H. Igel, and Y. Ben-Zion (1991). Observation and modeling of fault zone seismic trapped waves in aid of precise precursory microearthquake location and evaluation, *Proc. Conf. Earthquake Prediction: State-of-the-Art,* Strasbourg, France, Oct. 15–18, 1991.

Li, Y.-G., P. C. Leary, and K. Aki (1987). Observation and modeling of fault-zone fracture seismic anisotropy. II. P-wave polarization anomalies, *Geophys. J. R. Astr. Soc.* **91,** 485–492.

Li, Y.-G. and P. C. Leary (1990). Fault zone trapped seismic waves, *Bull. Seism. Soc. Am.* **80,** 1245–1271.

Li, Y.-G., P. Leary, K. Aki, and P. Malin (1990). Seismic trapped modes in the Oroville and San Andreas fault zones, *Science* **249,** 763–766.

Li, Y.-G, K. Aki, D. Adams, A. Hasemi, and W. H. K. Lee (1994a). Seismic guided waves trapped in the fault zone of the Landers, California, earthquake of 1992, *J. Geophys. Res.* **99,** 11705–11725.

Li, Y.-G., J. E. Vidale, K. Aki, C. Marone, and W. H. K. Lee (1994b). Fine structure of the Landers fault zone; segmentation and the rupture process, *Science* **256,** 367–370.

Lindh, A. and D. M. Boore (1974). The relation of the Parkfield foreshocks to the initiation and extent of rupture (abstract), *Earthquake Notes* **45,** 54.

Louie, J. N., R. J. L. Bras, and R. W. Clayton (1988). Three-dimensional imaging of steeply dipping structure near the San Andreas fault, Parkfield, California, *Geophysics* **53,** 176–185.

McNally, K. C. and T. V. McEvilly (1977). Velocity contrast across the San Andreas fault in central California; small-scale variations from P-wave nodal plane distortion, *Bull. Seism. Soc. Am.* **67,** 1565–1576.

Michael, A. J. and D. Eberhart-Philips (1991). Relations among fault behavior, subsurface geology, and three-dimensional velocity models, *Science* **253,** 651–654.

Michelini, A. and T. V. McEvilly (1991). Seismological studies at Parkfield. I. Simultaneous inversion for velocity structure and hypocenters using cubic B-splines parameterization, *Bull. Seism. Soc. Am.* **81,** 524–552.

Mooney, W. D. and A. Ginzburg (1986). Seismic measurements of the internal properties of fault zones, *Pure Appl. Geophys.* **124,** 141–157.

Nicholson, C. and J. M. Lees (1992). Travel-time tomography in the northern Coachella Valley using aftershocks of the 1986 M_L 5.9 North Palm Springs earthquake, *Geophys. Res. Lett.* **19,** 1–4.

Scholz, C. H. (1990). The mechanics of earthquakes and faulting, Cambridge University Press, Cambridge, 439 pp.

Sibson, R. H. (1973). Interactions between temperature and pore fluid pressure during earthquake faulting—a mechanism for partial or total stress relief, *Nature* **243,** 66–68.

Sibson, R. H. (1977). Fault rocks and fault mechanisms, *J. Geol. Soc. London* **133,** 191–213.

Vidale, J. E. and D. H. Helmberger (1987). Path effects in strong motion seismology, in *Methods of Computational Physics,* Vol. 11, Bruce Bolt (Editor) (entitled *Seismic Strong Motion Synthetics*), Academic Press, London, 217–317.

Vidale, J. E. (1988). Finite-difference calculations of travel times in three dimensions, *Bull. Seism. Soc. Am.* **78,** 2062–2076.

Vidale, J. E. (1990). Comment on "A comparison of finite-difference and Fourier method calculations of synthetic seismograms" by C. R. Daudt *et al., Bull. Seism. Soc. Am.* **80,** 493–495.

Vidale, J. E., D. V. Helmberger, and R. W. Clayton (1985). Finite-difference seismograms for SH waves, *Bull. Seism. Soc. Am.* **75,** 1765–1782.

Wald, D. J. and T. H. Heaton (1994). Spatial and temporal distribution of slip for the 1992 Landers, California, earthquake, *Bull. Seism. Soc. Am.* **84,** 668–691.

Wang, C. Y. (1984). On the constitution of the San Andreas fault zone in central California, *J. Geophys. Res.* **89,** 5558–5866.

Department of Earth Sciences
University of Southern California
Los Angeles, California 90089-0740
(Y.-G. L.)

U. S. Geological Survey, MS 977
Menlo Park, California 94025
(J. E. V.)

Manuscript received 21 March 1995.